

Research Article

The thioredoxin-1 and glutathione/glutaredoxin-1 systems redundantly fuel murine B-cell development and responses

Jonathan Muri¹, Helen Thut¹, Sebastian Heer¹, Caroline C. Krueger², Georg W. Bornkamm³, Martin F. Bachmann² and Manfred Kopf¹ 

¹ Institute of Molecular Health Sciences, ETH Zurich, Zürich, Switzerland

² Department of BioMedical Research, University of Bern, Department of Immunology RIA, University Hospital Bern, Bern, Switzerland

³ Institute of Clinical Molecular Biology and Tumor Genetics, Helmholtz Zentrum München, München, Germany

Antioxidant systems maintain cellular redox homeostasis. The thioredoxin-1 (Trx1) and the glutathione (GSH)/glutaredoxin-1 (Grx1) systems are key players in preserving cytosolic redox balance. In fact, T lymphocytes critically rely on reducing equivalents from the Trx1 system for DNA biosynthesis during metabolic reprogramming upon activation. We here show that the Trx1 system is also indispensable for development and functionality of marginal zone (MZ) B cells and B1 cells in mice. In contrast, development of conventional B cells, follicular B-cell homeostasis, germinal center reactions, and antibody responses are redundantly sustained by both antioxidant pathways. Proliferating B2 cells lacking *Txnrd1* have increased glutathione (GSH) levels and upregulated cytosolic *Grx1*, which is barely detectable in expanding thymocytes. These results suggest that the redox capacity driving proliferation is more robust and flexible in B cells than in T cells, which may have profound implications for the therapy of B and T-cell neoplasms.

Keywords: Antibody responses · B cell development · Glutaredoxin-1 · Thioredoxin-1



Additional supporting information may be found online in the Supporting Information section at the end of the article.

Introduction

Maintaining cellular redox homeostasis is essential for life. This process continuously requires cytosolic disulfide reduction reactions to recycle oxidized proteins back into their reduced thiol forms. The pentose phosphate pathway (PPP) has the critical role to alternatively oxidize glucose to generate NADPH, which in turn provides the reducing equivalents for driving numerous anabolic and redox reactions in the cell [1]. In particular, NADPH acts as an

electron donor for the two main cellular antioxidant pathways: the thioredoxin (Trx) and the glutathione (GSH)/glutaredoxin (Grx) systems [2, 3]. The reducing power of both systems fuels and sustains several cellular redox processes, including the synthesis of new DNA building blocks by ribonucleotide reductase (RNR), the detoxification of reactive oxygen species (ROS), and the reduction of protein disulfides into their respective thiol forms [2, 4–7].

The Trx system comprises Trx reductase (TrxR, encoded by *Txnrd*), Trx, and the thioredoxin-interacting protein (Txnip), which binds to reduced Trx and blocks its functions [4, 8]. In the GSH/Grx system, glutathione reductase (Gsr) catalyzes the reduction of GSH disulfide (GSSG) to its sulfhydryl form (GSH), which can then further reduce oxidized Grxs [9]. In the cytoplasm of

Correspondence: Prof. Manfred Kopf
e-mail: Manfred.Kopf@ethz.ch

mammalian cells, TrxR1 and Trx1 of the Trx system fuel reduction reactions to maintain cytosolic redox balance. Similarly, Grx1 is a critical cytosolic Grx, also contributing to this task [4, 10]. Both the Trx and the GSH/Grx systems donate electrons to partially shared substrates, which results in overlapping bioactivities. For instance, both pathways have been described to provide reducing power to RNR [10, 11]. While the GSH/Grx system was demonstrated to be the most efficient electron donor for RNR in *E. coli* [12], the Trx system is the critical pathway to sustain RNR function in yeast [13]. Whether the Trx or the Grx system is the main player for fueling DNA synthesis in mammalian cells is less clear, although a functional redundancy has been described in several contexts when either one of the systems is compromised [10]. Global knock-out (KO) of *Txnrd1* results in embryonic lethality at E9.5±1 due to inability to form the primitive streak mesoderm and general growth retardation, consistent with the impaired growth of embryonic fibroblasts in vitro [14, 15]. We have recently demonstrated that the Trx1 system plays a pivotal role in fueling DNA biosynthesis by donating reducing equivalents to RNR in proliferating T lymphocytes [16]. When this system is compromised by *Txnrd1* deletion, expansion of thymocytes during development and proliferation of T cells during immune responses is completely abrogated, thereby indicating that the GSH/Grx system cannot compensate for the absence of the Trx system in T cells [16]. Notably, cardiomyocytes develop normally in the absence of *Txnrd1* [15], implying that the GSH/Grx system can compensate for the absence of the Trx system. Also, growth of *Txnrd1*-deficient hepatocytes has been suggested to rely on the reducing power from the GSH/Grx system [17]. Interestingly, however, hepatocytes can develop in the absence of both *Txnrd1* and Gsr by NADPH-independent glutathione synthesis using the reducing power of dietary methionine [18, 19]. To which extent, however, the Trx and GSH/Grx systems can compensate for each other's functions in vivo is poorly understood at present.

Lymphocytes can undergo activation, grow, proliferate, perform effector functions, and return to a resting state. These fundamental processes are strictly dependent on dynamic changes in cellular metabolism [20]. Although naïve T cells primarily oxidize glucose-derived pyruvate in their mitochondria using oxidative phosphorylation (OXPHOS), activated T cells engage a program of aerobic glycolysis in order to allow anabolic growth and biomass accumulation [21, 22]. We have shown that the transcription factor c-Myc activates the Trx system during T-cell metabolic reprogramming to generate reducing power for the synthesis of new DNA building blocks [16]. *Txnrd1*-deficient T cells fail to develop in the thymus and to expand during in vivo viral and parasite infections due to impaired nucleotide biosynthesis [16]. B cells, the other main type of lymphocyte, also undergo metabolic reprogramming upon activation, but their metabolic changes have been poorly investigated in comparison to T cells. Whereas B cells also increase glycolysis after activation, like T cells, the metabolic basis of the unique features of B cells, including antibody production, class switching, and affinity maturation, is not fully understood [23–25]. Considering the critical role of the Trx1 system in T-cell metabolic reprogramming, in this study, we investigated

the function of this antioxidant system during B-cell development, germinal center (GC) reactions, and in vivo antibody responses. We surprisingly found that, unlike T cells, B cells have a functional GSH/Grx system, which is sufficient to catalyze cellular thiol-based redox reactions in the absence of the Trx system. Indeed, *Txnrd1* was dispensable for bone marrow development and its deletion only led to a partial delay in GC reactions and antibody production. These results consequently indicate that the cellular antioxidant system of B lymphocytes is flexible and robust, and they suggest that only dual targeting of both the Trx and GSH/Grx systems might be efficient against B-cell malignancies.

Results

Txnrd1 is dispensable for B-cell development

We have previously established a pivotal role of the Trx1 system in thymocyte proliferation and expansion of activated T cells [16]. We next wondered whether B cells are also dependent on the Trx1 system for development and function. To address this question, we generated *Txnrd1^{fl/fl};Cre-ERT2* mice by crossing mice with loxP-flanked *Txnrd1* alleles to mice carrying tamoxifen (TAM)-inducible *Cre-ERT2*. In these mice, *Txnrd1* gene deletion is achieved by TAM injection. Cre-mediated deletion in B cells of *Txnrd1^{fl/fl};Cre-ERT2* mice was complete at the genomic DNA and mRNA level in bone marrow and splenic CD19⁺ B cells upon TAM administration (Fig. 1A and B). Surprisingly, the frequency and number of CD19⁺IgM⁻, CD19⁺IgM⁺, and CD19⁺IgM⁺ cells were comparable in the bone marrow of TAM-treated *Txnrd1^{fl/fl};Cre-ERT2*, and control (*Txnrd1^{fl/fl}*) mice (Fig. 1C and D). Moreover, *Txnrd1* deficiency did not affect the number of CD19⁺ B cells in the periphery, including the spleen, lymph nodes, blood, liver, and lungs (Fig. 1E–I). By contrast, TAM injection into *Txnrd1^{fl/fl};Cre-ERT2* mice led to a massive reduction in total thymocytes (Fig. 1J), consistent with a pivotal role of *Txnrd1* in thymocyte expansion [16]. Taken together, these data indicate that the Trx1 system plays a crucial role in thymic T-cell expansion but is largely dispensable for B-cell development and homeostasis, implying distinct requirements of antioxidant pathways between B and T lymphocytes.

Txnrd1 is critical for MZ but dispensable for follicular B cells

To further study the striking difference in the requirement of the Trx1 system between B and T lymphocytes, we generated *Txnrd1^{fl/fl};Cd19-Cre* mice. Expectedly, deletion of *Txnrd1* occurred early during bone marrow development at the pro-B cell stage, thereby leading to a B-cell specific KO for *Txnrd1*. Efficient Cre-mediated deletion of *Txnrd1* was confirmed in CD19⁺ cells in bone marrow, spleen, and lungs at the genomic DNA and mRNA level (Fig. 2A and B). We next studied B-cell development in the bone marrow by flow cytometry using the *Hardy* classification system [26] comprising fraction A (pre/pro-B cells), fraction B

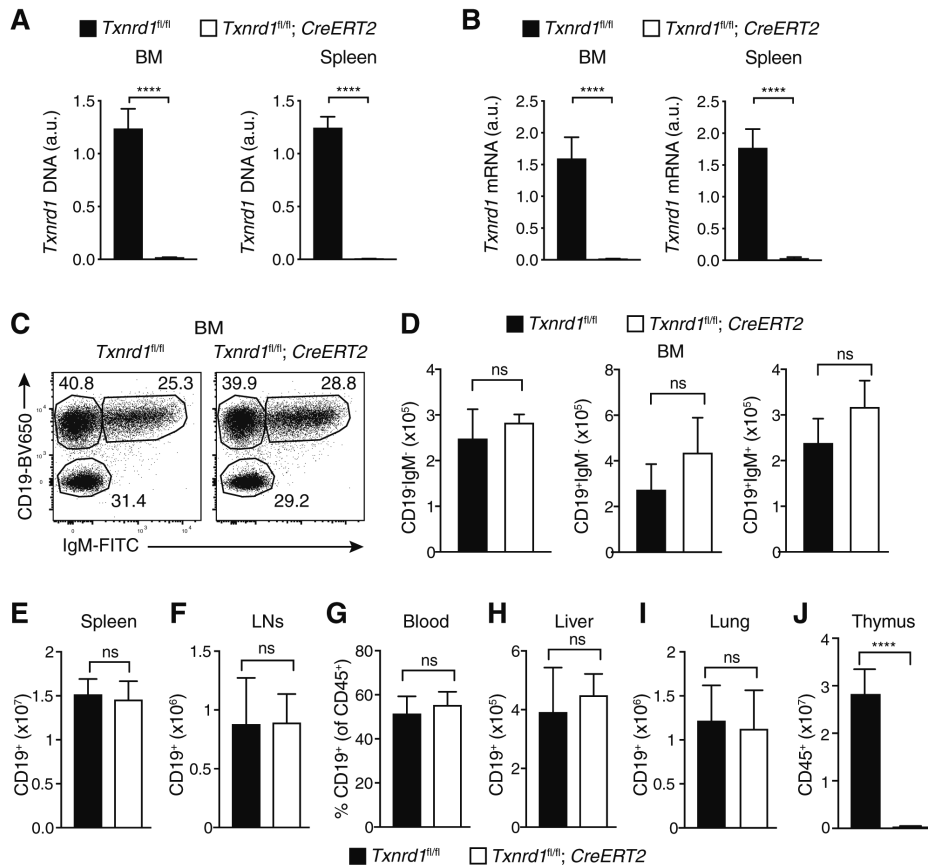


Figure 1. *Txnrd1* is required for the development and maintenance of T cells but not B cells. *Txnrd1^{fl/fl}; Cre-ERT2* mice and control *Txnrd1^{fl/fl}* littermates were injected with TAM to delete the *Txnrd1* gene and were analyzed by flow cytometry 2 weeks later ($n = 4-5$). (A, B) Analysis of genomic *Txnrd1* DNA (A) and *Txnrd1* mRNA (B) in MACS-enriched CD19⁺ cells from the bone marrow (BM; left) and spleen (right) by real-time PCR. (C, D) Representative FACS plots (C) and quantification (D) of CD19⁻IgM⁻, CD19⁺IgM⁻, and CD19⁺IgM⁺ populations in the BM. (E–I) Total B-cell numbers in the spleen (E), inguinal lymph nodes (F), blood (G), liver (H), and lung (I). (J) Absolute cell counts of total CD45⁺ thymocytes. Bar graphs show mean + standard deviation. Numbers in the FACS plots indicate the percentage of the depicted gates. Data are representative of two (A, B) and three (C–J) independent experiments. Student's *t* test (two-tailed, unpaired) was used to compare *Txnrd1^{fl/fl}* and *Txnrd1^{fl/fl}; Cre-ERT2* groups (A, B, D–J): * $p \leq 0.05$; ** $p \leq 0.01$; *** $p \leq 0.001$; **** $p \leq 0.0001$; ns, not significant.

(pro-B cells), fraction C (large pre-B cells), fraction D (small pre-B cells), fraction E (immature B cells), and fraction F (mature B cells). *Txnrd1* deficiency did not affect total numbers of B-cell precursors in any of these fractions (Fig. 2C), which, together with the results above, demonstrates that the Trx system is dispensable for the bone marrow development of B lymphocytes. We next compared proliferation in the bone marrow and in the thymus by measuring incorporation of the thymidine analog 5-Ethynyl-2'-deoxyuridine (EdU). Notably, B-cell precursors of fraction C proliferated even more vigorously than CD44⁺CD25⁺ (DN2) and CD44⁻CD25⁻ (DN4) thymocytes, suggesting that dispensability of *Txnrd1* in B cells cannot be explained by a slower proliferation rate (Fig. 2D).

Newly formed B cells emigrate from the bone marrow to the spleen where they undergo final maturation by further differentiating into either CD23⁺ follicular or CD21/35⁺CD23⁻ marginal zone (MZ) B cells, both belonging to the B2 cell compartment [27]. Interestingly, MZ B cells but not follicular B cells lacking TrxR1 were significantly reduced in the spleen (Fig. 2E–H). Moreover, B-cell numbers in the lymph nodes (Fig. 2I) and blood (Supporting Information Fig. 1A) as well as their activation status as determined by measurement of CD62L surface expression remained unaffected in the absence of the Trx1 system (Fig. 2J, Supporting Information Fig. 1B). Also, fraction C pre-B cells in the bone marrow showed normal proliferation (i.e. EdU incorporation; Supporting Information Fig. 1C). To further assess the requirement of the Trx1 system in a competitive situation with WT cells, we generated

mixed-bone marrow chimeras by reconstituting lethally irradiated C57BL/6 mice (CD45.1⁺CD45.2⁺) with an equal ratio of congenically marked donor bone marrow cells from WT (CD45.1⁺) and *Txnrd1^{fl/fl}; Cd19-Cre* (CD45.2⁺) or *Txnrd1^{fl/fl}* (CD45.2⁺) mice as control. Consistent with the previous results, *Txnrd1*-deficient B cells were able to contribute similarly to all developmental stages of B-cell lymphopoiesis as control B cells (Fig. 2K). In this setting, however, *Txnrd1*-deficient MZ B cells were outcompeted by *Txnrd1*-sufficient cells to a higher proportion compared to follicular B cells (Fig. 2L). Taken together, these data indicate that the Trx1 system is largely dispensable for the development of B cells in the bone marrow and for the generation of follicular B cells in the spleen, but it plays a critical role for the differentiation/maintenance of MZ B cells.

B1 cells are critically dependent on *Txnrd1* for development and responses

B cells can be subdivided into B1 and B2 cells. Although both MZ and follicular B cells belong to the B2 population, they are functionally distinct. Indeed, MZ B cells rapidly respond to blood-borne antigens with T cell-independent antibody production, thereby resembling B1 rather than follicular B cells [28]. Since the Trx1 system appears to be critical for MZ B cells, we next assessed its role in B1 cells. In the peritoneal cavity, which constitutes the main B1 cell reservoir, we found reduced frequency and total

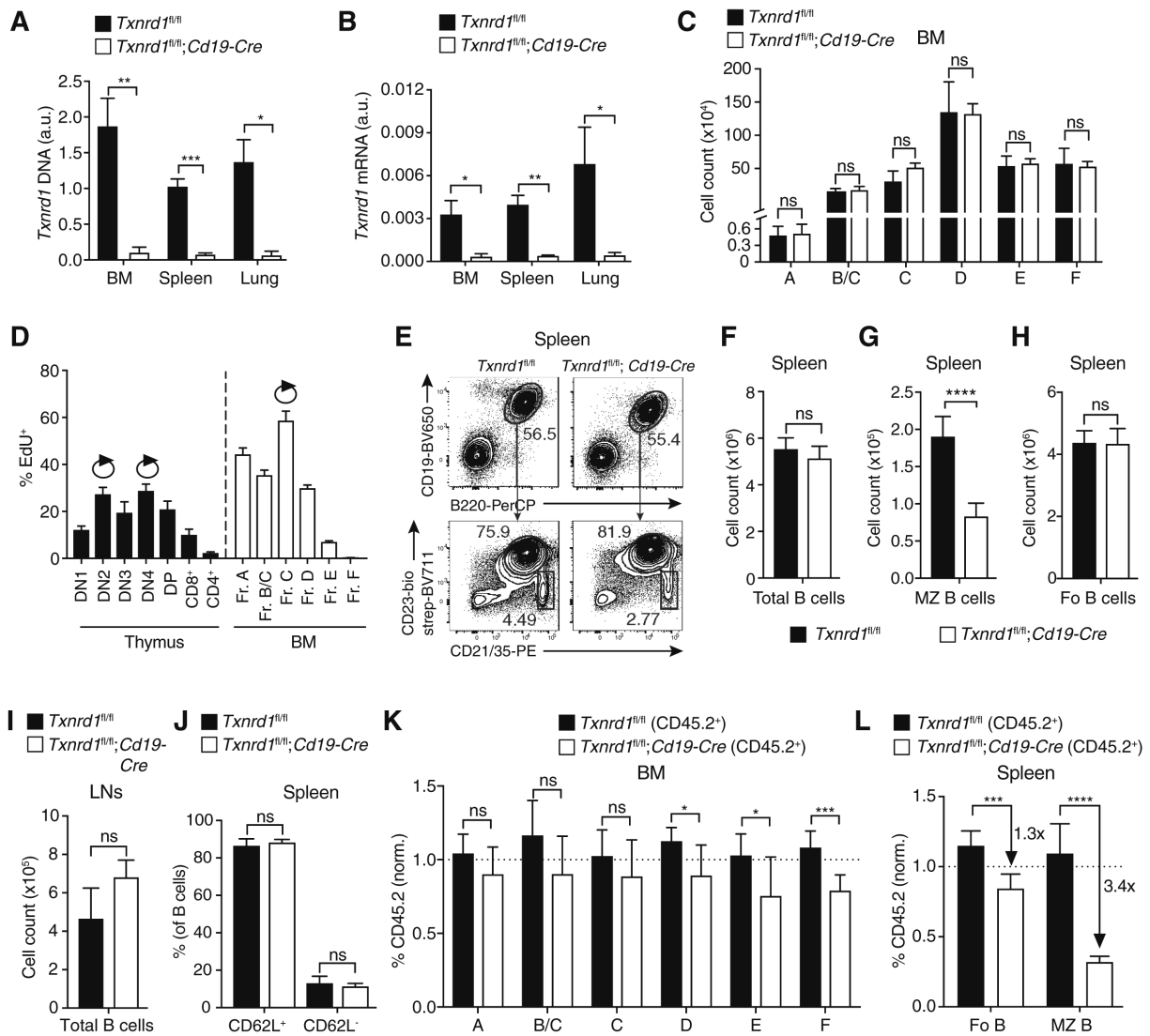
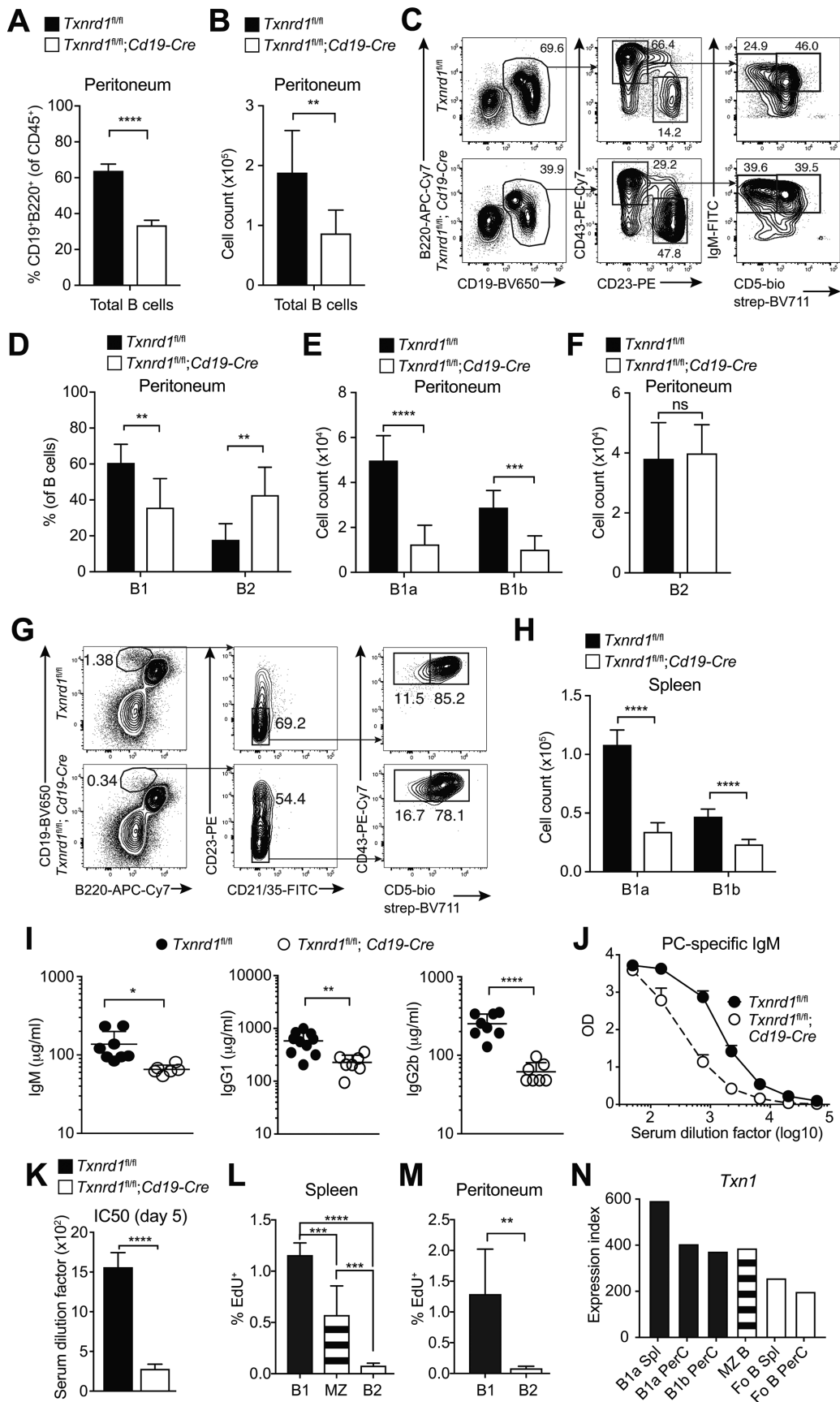


Figure 2. *Txnrd1* is critical for MZ but dispensable for follicular B-cell development and homeostasis. Analysis of the different B-cell populations in naive *Txnrd1^{fl/fl};Cd19-Cre*, and *Txnrd1^{fl/fl}* littermate control mice. (A, B) Genomic *Txnrd1* DNA (A) and *Txnrd1* mRNA (B) in MACS-enriched CD19⁺ cells from the bone marrow (BM), spleen, and lungs by real-time PCR ($n = 3$). (C) The quantifications of the indicated Hardy B cells fractions are shown ($n = 4-6$). (D) Proliferation of CD25⁻CD44⁺ (DN1), CD25⁺CD44⁺ (DN2), CD25⁺CD44⁻ (DN3), CD25⁻CD44⁻ (DN4), CD4⁺CD8⁺ (DP), CD4⁺, and CD8⁺ thymocytes (left), and of the indicated Hardy B-cell populations (right) was assessed by EdU incorporation. Circular arrows indicate highly proliferating populations ($n = 5$). (E) Gating strategy of follicular (CD23⁺) and MZ (CD21/35⁺CD23⁻) B cells in the spleen. Numbers in the FACS plots indicate the percentage of the depicted gate. (F-I) Absolute cell counts of total B cells (F), MZ B cells (G), and follicular (Fo) B cells (H) in the spleen, and of total B cells in the inguinal lymph nodes (I; $n = 6$). (J) Expression of CD62L on splenic CD19⁺ B cells ($n = 5-6$). (K-L) Lethally irradiated WT mice were reconstituted with a 1:1 mixture of WT and *Txnrd1^{fl/fl};Cd19-Cre* (or *Txnrd1^{fl/fl}* as control) BM expressing the congenic markers CD45.1 and CD45.2, respectively. After reconstitution, the contribution of *Txnrd1^{fl/fl};Cd19-Cre* cells to the indicated populations in the BM (K) and spleen (L) was assessed. Values were normalized to non-Cre expressing CD45.2⁺TCR β ⁺ T cells. Values below 1 indicate reduced contribution of *Txnrd1*-deficient B cells compared to WT cells ($n = 6$). Bar graphs show mean + standard deviation. Numbers next to the arrows indicate fold-changes between the groups (L). Data are representative of two (A, B, D, I-L) and three (C, E-H) independent experiments. Student's *t* test (two-tailed, unpaired) was used to compare *Txnrd1^{fl/fl}* and *Txnrd1^{fl/fl};Cd19-Cre* groups (A, B, C, F-L): * $p \leq 0.05$; ** $p \leq 0.01$; *** $p \leq 0.001$; **** $p \leq 0.0001$; ns, not significant.

number of CD19⁺ B cells in *Txnrd1^{fl/fl};Cd19-Cre* mice (Fig. 3A-C). The frequency of B2 cells was increased in the peritoneum, while the frequency of B1 cells was reduced (Fig. 3C and D). B1 cells can be further separated into B1a and B1b cells according to the expression of CD5, which is a marker of B1a cells. *Txnrd1* deficiency led to dramatic reduction of both B1a and B1b cells (Fig. 3C and E), while the number of B2 cells remained unchanged

(Fig. 3F). Consistent with the reduction in the peritoneal cavity, we observed that B1a and B1b cells were also decreased in the spleen (Fig. 3G and H). B1 and MZ B cells have been demonstrated to be the main producers of natural antibodies [29]. Consistent with reduction of these B-cell subsets in naive *Txnrd1^{fl/fl};Cd19-Cre* mice, we found impaired levels of natural IgM, IgG1, and IgG2b antibodies compared to control mice (Fig. 3I). In addition



to providing a first line of defense with natural antibody production, B1 and MZ B cells are also indispensable for mounting low-affinity phosphorylcholine (PC)-specific IgM antibody responses to *S. pneumoniae* reaching the blood [28, 30, 31]. Thus, we immunized mice with heat-inactivated bacteria intravenously and measured specific IgM antibody response after 5 days. Whereas control mice mounted a strong anti-PC IgM response, *Txnrd1^{fl/fl};Cd19-Cre* mice had strongly reduced PC-specific IgM titers (Fig. 3J and K). Together, these findings show that the Trx1 system is necessary for the development and function of MZ and B1 cells but dispensable for B2 cells.

It is well established that B1 cells are maintained by self-renewal rather than de novo development, in contrast to B2 cells [28, 32]. We thus speculated that the critical requirement of the Trx1 system in B1 cells could be due to the continuous proliferation they undergo in order to maintain a stable population size over time. To investigate this, we compared EdU incorporation in follicular B, MZ B, and B1 cells at the steady state. Indeed, we observed that B1 cells proliferated more than B2 cells in the spleen and in the peritoneal cavity, and that splenic MZ B cells also expanded more than follicular B2 cells (Fig. 3L and M). Moreover, B1 and MZ B cells expressed higher levels of *Txn1* compared to follicular B cells (Fig. 3N), implying that these cells mostly rely on the Trx1 system for thiol-based redox reactions. Overall, these results suggest that *Txnrd1* is critical for B1 and MZ B cells cycling during homeostatic proliferation.

The GSH/Grx system sustains proliferation of developing B cells in the absence of the Trx1 system

We have recently shown that thymic T-cell proliferation is licensed by a high *Txnrd1*-*Txn1* to *Txnip* ratio [16]. To evaluate this in B-cell development, we compared the mRNA levels of *Txnrd1*, *Txn1*, and *Txnip* using the Immgen database. Similar to proliferating thymocytes, we observed that the highly cycling pre-B cells from the Hardy fraction C are associated with low levels of *Txnip* but high levels of *Txn1* and *Txnrd1* (Fig. 4A, Supporting Information Fig. 2A), suggesting that the Trx1 system might sustain RNR function during B-cell development like in T cells. However, B-cell development was normal in the absence of *Txnrd1* (Figs. 1 and 2). Compensatory activity of the Trx and GSH/Grx systems

has been reported [10, 17]. Interestingly, we observed that Grx1, the main cytosolic Grx, was upregulated in *Txnrd1*-deficient bone marrow B cells, while the other Grx isoforms remained unchanged (Fig. 4B), implying that cytosolic Grx1 might compensate for the absence of the Trx1 system and fuel its reducing power to RNR for DNA biosynthesis. In line with this, we observed that the Hardy fraction C pre-B cells contained significantly higher levels of cellular GSH in the absence of the Trx system, whereas the other Hardy fractions only displayed a trend to increased GSH levels (Fig. 4C). Fraction C is indeed the highest cycling fraction in the bone marrow and therefore requires more reducing power to sustain DNA biosynthesis and other thiol-based redox reactions. Similar results were also obtained by measuring total GSH levels in CD19⁺ bone marrow cells (Fig. 4D).

To address the role of the alternative GSH/Grx1 system in B-cell development, we used L-buthionine-sulfoximine (BSO) to inhibit glutamate-cysteine ligase and block GSH synthesis [33] (Fig. 4E). Oral administration of the compound can effectively deplete GSH levels in vivo [34]. Accordingly, BSO-treatment reduced the cellular GSH pool in bone marrow cells of both *Txnrd1^{fl/fl}* and *Txnrd1^{fl/fl};Cd19-Cre* mice (Fig. 4F and G). Although no effects were observed in the Hardy fractions B-C, GSH depletion led to reduced B-cell numbers in the fractions D-F in *Txnrd1^{fl/fl};Cd19-Cre* mice (Fig. 4H). This is in line with the requirement of reducing power to fuel RNR function in highly proliferating pre-B cells of the fraction C, which do not efficiently develop into the subsequent fractions when both the Trx1 and GSH/Grx systems are compromised. Furthermore, BSO-treatment did not affect B-cell development at any stage in WT *Txnrd1^{fl/fl}* mice, indicating that GSH/Grx1 is not the predominant redox system in B-cell development. GSH depletion also did not affect expansion of thymocytes (Supporting Information Fig. 2B), which is driven by the Trx1 system [16].

Interestingly, *Txn1* expression is higher in thymocytes compared to bone marrow B cells (Fig. 4I). Conversely, *Grx1* mRNA was barely detectable at any stage of thymocyte development but expressed highly in bone marrow B cells (Fig. 4J, Supporting Information Fig. 2C). This is a likely explanation for why thymocytes cannot rely on the GSH/Grx1 system for proliferation when they lack *Txnrd1*.

Taken together, these data demonstrate that pre-B cells lacking TrxR can resort to the GSH/Grx1 system as an electron

Figure 3. *Txnrd1* is critical for MZ B- and B1-cell maintenance and responses. (A–H) B-cell populations in naïve *Txnrd1^{fl/fl};Cd19-Cre*, and *Txnrd1^{fl/fl}* littermate control mice were analyzed by flow cytometry. (A, B) Percentages (A) and absolute cell counts (B) of total CD19⁺B220⁺ B cells in the peritoneal cavity ($n = 6–8$). (C) Gating strategy for B1 (CD43⁺CD23⁻) and B2 (CD23⁺CD43⁻) cells in the peritoneal cavity. (D–F) Shown are the percentages of B1 and B2 cells (D), the cell counts of B1a and B1b cells (E), and the total numbers of B2 cells (F) in the peritoneal cavity ($n = 6–8$). (G, H) Gating strategy (G) and absolute cell numbers (H) of B1a and B1b cells in the spleen ($n = 6$). (I) Concentration of IgM (left), IgG1 (middle), and IgG2b (right) in the serum of naïve mice. Symbols represent individual mice. (J, K) *Txnrd1^{fl/fl};Cd19-Cre* and *Txnrd1^{fl/fl}* littermate control mice were infected with *S. pneumoniae*, and PC-specific IgM titers were determined by ELISA 5 days after immunization ($n = 5$). (J) Optical density (OD) values at day 5 upon *S. pneumoniae* infection. (K) IC50 for PC-specific IgM response 5 days after immunization. (L, M) Proliferation of the indicated B-cell populations in the spleen (L) and in the peritoneal cavity (M) was assessed by EdU incorporation ($n = 6$). (N) Shown are the mean expression values of *Txn1* in the indicated populations in the spleen and peritoneal cavity (PerC) obtained from the Immgen database. Bar graphs or dot plots show mean + standard deviation (A, B, D–F, H, I, K–M) or mean + standard error of mean (J). Numbers in the FACS plots indicate the percentage of the depicted gate. Data are representative of three (A–F, I) and two (G, H, J–M) independent experiments. Student's *t* test (two-tailed, unpaired) was used in A, B, D–F, H, I, K, M: * $p \leq 0.05$; ** $p \leq 0.01$; *** $p \leq 0.001$; **** $p \leq 0.0001$; ns, not significant. One-way ANOVA adjusted by Tukey's multiple comparison test was used in L: ** $p \leq 0.0332$; *** $p \leq 0.0021$; **** $p \leq 0.0002$.

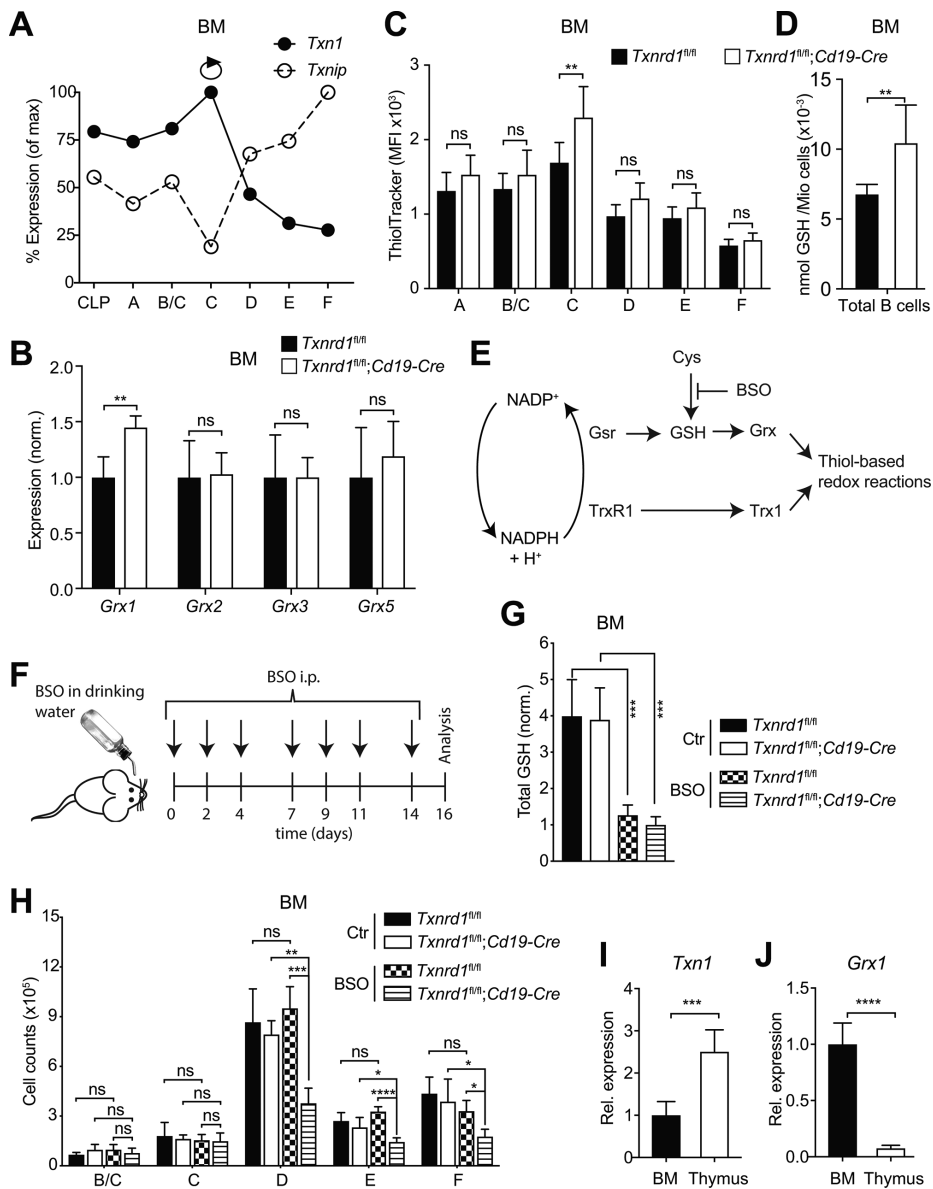


Figure 4. *Grx1* can take over the function of *Txn1* during B-cell development. (A) Mean expression values of *Txn1* and *Txnip* determined by microarray in the indicated bone marrow (BM) B-cell populations (from the Immgen database). The circular arrow indicates the highly proliferative population (Fraction C). (B) Expression of the indicated *Grx* isoforms in the BM determined by RT-PCR ($n = 5-6$). (C) Reduced thiols were detected with ThiolTracker reagent by flow cytometry to estimate cellular levels of reduced GSH ($n = 7-5$). (D) Total levels of GSH measured in cell lysates of MACS-sorted CD19⁺ cells from the BM ($n = 5-6$). (E) Schematic showing the two main cellular antioxidant pathways and the action of L-buthionine-sulfoximine (BSO). (F) Illustration of the *in vivo* animal model for continuous depletion of GSH by BSO administration. (G, H) *Txnrd1^{fl/fl};Cd19-Cre* and *Txnrd1^{fl/fl}* littermate control mice were administered with BSO to deplete glutathione (GSH) *in vivo* ($n = 4-6$). (G) Total glutathione (GSH) levels in the indicated total BM lysates. (H) B-cell populations in the BM were analyzed by flow cytometry. (I, J) Expression levels of *Txn1* (I) and *Grx1* (J) in the thymus and in the BM were determined by RT-PCR ($n = 5-6$). Letters A-F indicate the different B-cell stages according to the Hardy's classification system (A, C, H). Bar graphs show mean + standard deviation. Data are representative of two (B-D, G, H) and three (I, J) independent experiments. Student's *t* test (two-tailed, unpaired) was used to compare *Txnrd1^{fl/fl}* and *Txnrd1^{fl/fl};Cd19-Cre* groups (B-D, I, J): * $p \leq 0.05$; ** $p \leq 0.01$; *** $p \leq 0.001$; **** $p \leq 0.0001$; ns, not significant. One-way ANOVA adjusted by Tukey's multiple comparison test was used in G, H: * $p \leq 0.1234$; ** $p \leq 0.0332$; *** $p \leq 0.0021$; **** $p \leq 0.0002$.

donor for proliferation, indicating functional redundancy of the two systems during B-cell development, in contrast to T-cell development.

Txnrd1 deficiency causes delayed antibody responses and germinal center reactions

We have shown above that the Trx system is completely dispensable for development and homeostatic maintenance of follicular B cells in several organs (Fig. 1 and 2). We next wondered whether follicular B cells require the Trx1 system for GC and antibody responses. For this purpose, we took advantage of replication-defective Q β virus-like particles (Q β -VLPs) containing *E. coli* ssRNA. Q β -VLPs have been well characterized and described to trigger very rapid and vigorous antibody responses, comprising both T cell-independent IgM and T cell-dependent IgG B-cell

responses. Moreover, Q β -VLPs also induce formation of GC, hypermutations, affinity maturation, and B-cell memory, thereby providing a suitable *in vivo* model to study B-cell responses [35–38]. We immunized *Txnrd1^{fl/fl}* and *Txnrd1^{fl/fl};Cd19-Cre* mice with Q β -VLPs and determined antibody levels at various time points over 10 weeks. Expectedly, control mice mounted a potent-specific IgM and IgG2b response already at day 6, which was strikingly impaired in *Txnrd1^{fl/fl};Cd19-Cre* mice (Fig. 5A and B). To our surprise, however, no significant differences in Q β -specific IgG2b responses were observed 2 and 10 weeks after immunization (Fig. 5B). After 2 weeks, Q β -specific IgM antibodies were even higher in KO mice, probably because levels in WT were already declining (Fig. 5A). Taken together, these results indicate that the absence of the Trx1 system in B lymphocytes results in a delay in antibody response and isotype switch. This implies that the GSH/Grx system can partially compensate for the absence of the Trx1 system during GC reactions.

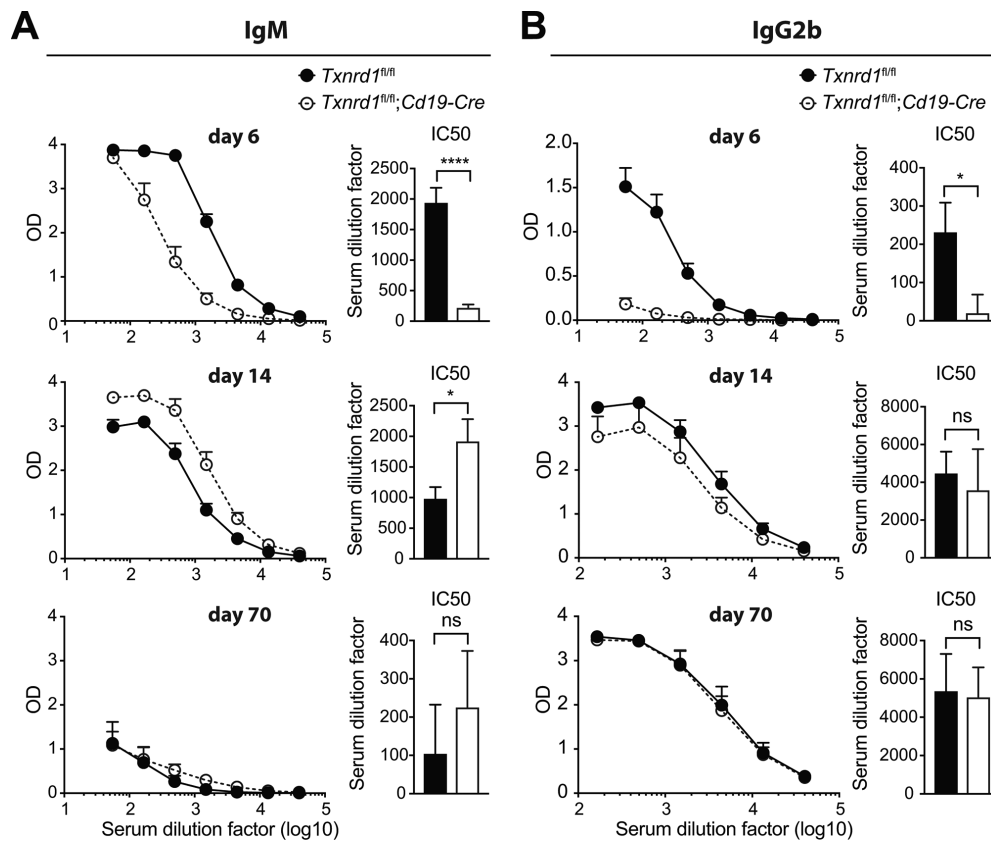


Figure 5. *Txnr1*-deficiency leads to delayed antibody responses in vivo. *Txnr1^{fl/fl};Cd19-Cre* and *Txnr1^{fl/fl}* littermate control mice were intraperitoneally immunized with Q β -VLPs containing *E. coli* ssRNA and bled at day 6 (top), 14 (middle), and 70 (bottom) after immunization in order to determine IgM (A) and IgG2b (B) antibody responses. Q β -VLP-specific IgM and IgG2b antibody titers were measured by ELISA. For each panel, plots of OD_{405nm} against serum dilutions (left) and IC₅₀ for Q β -VLP-specific antibodies (right) are shown. Dots in the plots and bar graphs represent mean + standard error of mean. Data are representative of three independent experiments. Student's *t* test (two-tailed, unpaired) was used to compare *Txnr1^{fl/fl}* and *Txnr1^{fl/fl};Cd19-Cre* groups (A, B): **p* \leq 0.05; *****p* \leq 0.0001; ns, not significant.

The observed delayed antibody response in the absence of the Trx1 system might arise from either a defect in antibody production/secretion or from a partially impaired expansion of follicular B cells in the GC. To address this, we analyzed formation of GCs in spleen sections by immunohistology. GC cells were identified by binding of peanut agglutinin (PNA), B-cell follicles by staining with an anti-B220 antibody, and antigen-specific cells using fluorophore-labeled Q β -VLP. Expectedly, *Txnr1^{fl/fl}* mice showed a few fully established GCs and clusters of Q β ⁺ centroblasts already at day 7 after immunization. At this time point, in *Txnr1^{fl/fl};Cd19-Cre* mice, we found a few isolated Q β ⁺ cells but no established GC, although structures with a few PNA⁺ cells that may develop into a GC were occasionally detectable (Fig. 6A and B). However, by day 12, no differences were observed in number and size of GCs and clusters of Q β ⁺ centroblasts when comparing WT and KO mice (Fig. 6A). Importantly, we verified that *Txnr1* deletion was complete in GC B cells (Supporting Information Fig. 3). These data are in line with the delayed antibody responses of mice lacking the Trx1 system (Fig. 5).

To further validate the immunohistology, we next analyzed B cells in the GC by flow cytometry. GC B cells possess the

typical cell-surface phenotype B220⁺CD38^{low}Fas⁺, and they can be further subdivided into dark zone (DZ) and light zone (LZ) cells based on the expression of the markers CXCR4 and CD86, respectively [39]. B220⁺CD38^{low}Fas⁺ GC B cells were about 17-fold reduced and barely detectable in the spleen of *Txnr1^{fl/fl};Cd19-Cre* mice in comparison to controls 7 days after Q β -VLP immunization (Fig. 6C and D). Despite the striking difference in total numbers of GC B cells, the distribution among LZ and DZ cells was comparable (Fig. 6E and F). Importantly, at day 12, the number GC B cells in the spleen of *Txnr1^{fl/fl};Cd19-Cre* mice have increased considerably and have almost reached the levels of WT controls (Fig. 6G). Taken together, these results indicate that B cells lacking the Trx1 system mount a delayed but, in the end, an efficient GC and B2-mediated antibody response.

To further investigate whether the delay in the antibody response has functional consequences in an infectious disease caused by a replicating virus, we infected *Txnr1^{fl/fl};Cd19-Cre* and control mice with influenza A virus (IVA) PR8. Indeed, infection with a low-dose of IVA resulted in much more severe disease course indicated by temperature and weight loss in the knockouts (Fig. 6H and I), which was due to a delayed

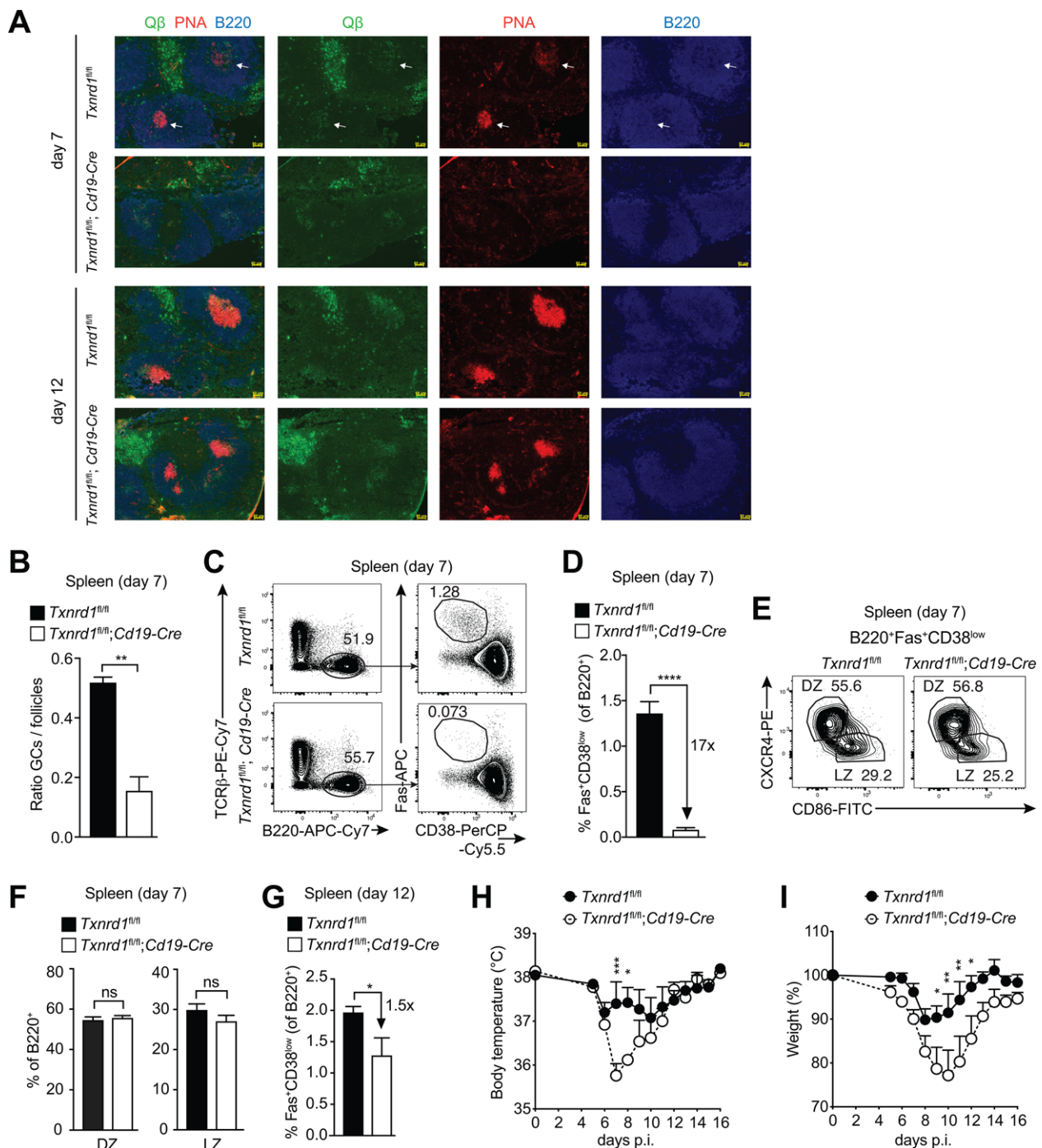


Figure 6. GC formation is delayed in the absence of the Trx1 system. (A–G) *Txnrd1^{fl/fl}; Cd19-Cre* and control *Txnrd1^{fl/fl}* littermates were intraperitoneally immunized with Q β -VLPs containing *E. coli* ssRNA. (A) Immunofluorescence of spleen sections 7 (top) and 12 (bottom) days after Q β -VLP immunization. Sections were stained with Q β -VLP (green), PNA (red), and anti-B220 antibody (blue). Scale bar represents 50 μ m. Arrows indicate mature GC structures at day 7. The images are representative of two mice per group, and 2–4 spleen sections were analyzed per mouse. (B) Quantification of the immunofluorescence data at 7 days after immunization. Depicted is the ratio between the total number of detected GCs and the numbers of identified follicles in two separate sections ($n = 2$ mice). (C, D) GC B cells in the spleen were analyzed by flow cytometry according to the expression of CD38 and Fas ($n = 4$ –5). (C) Representative FACS plots 7 days after Q β -VLP immunization. (D) Quantification of B220⁺CD38^{low}Fas⁺ GC B cells 7 days after challenge. (E, F) Light zone and dark zone B cells in the spleen at day 7 were gated according to the expression of CXCR4 and CD86. Representative FACS plots (E) and quantification (F) of CXCR4⁺CD86⁺ (LZ) and CXCR4⁺CD86⁻ (DZ) B cells are shown ($n = 3$). (G) Quantification of B220⁺CD38^{low}Fas⁺ GC B cells 12 days after challenge ($n = 4$ –5). (H–I) *Txnrd1^{fl/fl}; Cd19-Cre* and *Txnrd1^{fl/fl}* littermate control mice were infected with 10 pfu PR8 influenza A virus. Weight (H) and temperature (I) relative to the day of infection are shown ($n = 4$ –5). Bar graphs show mean + standard deviation (B, D, F, G). Dot plots represent mean + standard error of mean (H, I). Data are representative of two independent experiments. Student's *t* test (two-tailed, unpaired) was used in B, D, F, G: * $p \leq 0.05$; **** $p \leq 0.0001$. Two-way ANOVA adjusted by Bonferroni's multiple comparison test was used in H, I: * $p \leq 0.1234$; ** $p \leq 0.0332$; *** $p \leq 0.0021$.

PR8-specific antibody response (Supporting Information Fig. 4A). Similar to VLP-induced antibody responses, *Txnrd1^{fl/fl}*; *Cd19-Cre* mice mounted a comparable antibody response late after low dose IVA infection, which was sufficient to protect from infection with a lethal dose of IVA (Supporting Information Fig. 4B). These data indicate that despite the delayed onset of the germinal center response in the absence of TrxR1, the generated antibodies possess neutralizing capacity.

Discussion

Immunometabolism has come of age by the demonstration that metabolic cues critically regulate T-cell and macrophage responses. Naïve T cells have low metabolic requirements and predominantly use OXPHOS to generate ATP. Upon activation, however, T cells adopt an anabolic metabolism aimed at biomass accumulation. This is achieved by engaging aerobic glycolysis, which has a key role in providing biosynthetic intermediates for the generation of fatty acids and nucleotides. For example, glucose-6-phosphate can be metabolized in the PPP to generate riboses for nucleotide synthesis [21, 40–43]. We have previously shown that the Trx1 system is critically activated by c-Myc during T-cell metabolic reprogramming, providing the reducing power to RNR at the last step of nucleotide biosynthesis. In the absence of the Trx1 system, T cells have reduced availability of 2'-deoxyribonucleotides, leading to replication stress, cell-cycle arrest, and compromised expansion [16]. While B cells share various metabolic features with T cells, such as their induction of aerobic glycolysis and increased glucose uptake upon activation [23, 24, 44], little is known about how metabolic changes dictate the fate of B cells during development, GC reactions, and antibody production. In recent years, it has become clear that cellular antioxidant pathways also regulate the metabolic changes of immune cells during *in vivo* responses [16, 45]. In this study, we investigated the role of the two main cellular antioxidant pathways (the Trx1 and GSH/Grx systems) in B-cell-mediated immunity. We have demonstrated that B cells, unlike T cells, can use both systems to support thiol-based redox reactions, such as the reduction of ribonucleotides into 2'-deoxyribonucleotides by RNR. This suggests that both systems are key players in B-cell metabolic reprogramming.

We found that in the absence of TrxR, the GSH/Grx system is sufficient to drive B-cell development in the bone marrow and maintain homeostasis of follicular B cells. Conversely, blockage of the GSH/Grx pathway did not affect B-cell development and peripheral homeostasis in the presence of TrxR. Thus, Trx and Grx are redundant in the delivery of reducing equivalents for the reduction reaction catalyzed by RNR during nucleotide biosynthesis. Among the different Grx isoforms, the cytosolic Grx1 is upregulated in *Txnrd1*-deficient B cells. Moreover, GSH levels were also increased in the absence of the Trx1 system, suggesting that *Txnrd1*-deficient B lymphocytes rearrange their redox system toward the GSH/Grx1 pathway in order to fuel thiol-based cellular redox reactions and to maintain redox homeostasis. Despite

the slower kinetics, we also found that B cells lacking the Trx system can expand, produce antibodies, give rise to GC structures and undergo class switching. Moreover, the antibodies produced by *Txnrd1*-deficient B cells late during primary influenza infection provide full protection upon rechallenge with a lethal dose of IVA, which may indicate that the antibodies are virus-neutralizing and have undergone normal affinity maturation. The delayed GC formation in *Txnrd1*-deficient B cells could on the one hand be explained by the fact that the Grx system might be less efficient than the Trx system in providing reducing equivalents to RNR. On the other hand, switching the antioxidant system from a mainly Trx-driven towards a Grx-driven system might require time, which would also cause a delay in GC reactions. This delay can be fatal upon infection with a lytic virus that must be controlled rapidly such as influenza virus, as demonstrated by our results above. The reduction of MZ B cells in naïve mice might also contribute to the defects observed in the early immune response, since the MZ B cell compartment has also been described to be capable of generating variable and diverse antibody responses [46]. The compensatory mechanism by the GSH/Grx1 system is absent in T cells, since *Txnrd1*-deficient T cells do not develop in the thymus and cannot proliferate during viral infections *in vivo* [16]. In line with this, we also found that proliferating thymocytes express high levels of Trx1 but almost undetectable levels of Grx1, while *Txnrd1*-deficient B cells in the bone marrow upregulated expression of Grx1 to adequately sustain cytosolic redox homeostasis.

In contrast to follicular B cells, we found that homeostatic maintenance of MZ and B1 cells was dependent on the Trx1 system. Although MZ B cells belong to the B2 cell lineage, they are functionally related to B1 cells due to their ability to rapidly respond to blood-borne antigens and to produce antibody without the help of T cells [28]. Our results demonstrated that *Txnrd1*-deficient MZ and B1 cells are already reduced in the steady-state, and consequently *Txnrd1^{fl/fl}*; *Cd19-Cre* mice have reduced natural antibody titers and cannot properly mount a PC-specific IgM antibody response to *S. pneumoniae* reaching the blood. Consistent with other reports [28, 32], we showed that B1 and MZ B cells undergo higher homeostatic proliferation in comparison to follicular B2 cells, which only barely cycle at steady state. Therefore, we speculate that the Trx1 system is required for the maintenance of B1 and MZ B cells, due to their increased cycling. In line with this, we also observed increased *Txn1* expression levels in B1 and MZ B cells compared to follicular B2 cells, also indicating a higher dependency on the Trx1 system.

Compared to T cells, which are critically dependent on the Trx pathways for development and responses, B cells are more flexible and can tap both pathways to ensure redox remodeling when one of them is inadequate. B cells are exposed to higher levels of ROS compared to T cells, which evolutionarily may explain the requirement for a more robust antioxidant system to maintain cytosolic redox balance. NADPH oxidases (NOX), which are expressed and used for microbial killing in granulocytes and macrophages, are also important contributor to ROS in B cells but not T cells. Among various NOX enzymes, B cells express NOX2 and dual oxidase 1 (DUOX1) [47]. Interfering with NOX2 activity in B cells

leads to a reduction of cellular ROS, thereby affecting B-cell activation, differentiation, and antibody responses [47]. Moreover, B cells have the unique capacity to secrete enormous amounts of antibodies. Folding and assembly of immunoglobulin molecules is known to involve numerous intra- and intermolecular disulfide bond formations, thereby leading to a biochemical cascade generating a flux of ROS from the endoplasmic reticulum [48]. This is in line with studies showing that components of cellular antioxidant pathways, including Nrf2, are increased during plasma cell differentiation [47, 49]. The fact that B cells generate large amount of ROS upon activation is consistent with our results and explains why they need such a robust cellular redox system.

Aberrant redox signaling underlies several human diseases, such as cancer. Numerous studies have reported that Trx and TrxR are upregulated in several types of cancers, including B-cell malignancies and aggressive T-cell acute lymphoblastic leukemia (T-ALL), and are associated with a poor clinical outcome of the patients. Notably, the Trx system is essential for tumor development, propagation, and metastasis, and is thought to be linked to resistance to chemotherapies [50–52]. The literature suggests that TrxR is involved in all the hallmarks of cancer described by Hanahan and Weinberg [53], such as inhibition of apoptosis, insensitivity to growth-inhibitory signals, limitless replicative potential, and sustainment of angiogenesis [50]. Therefore, it is not surprising that various chemotherapeutic drugs have been developed to target TrxR, mostly by induction of apoptosis or oxidative stress [54, 55]. The gold-based drug auranofin inhibits TrxR and can induce apoptosis of various human tumors, such as ovarian cancer [56], breast cancer [57], and multiple myeloma [58]. Genetic deficiency and/or pharmacological inhibition of both the GSH and Trx pathways synergistically mediates cell death of cancer cells *in vitro* and *in vivo* [59, 60], indicating that these two antioxidant systems are critical for tumor progression and can partially compensate for each other. A recent study revealed that dual targeting of the Trx and GSH systems blocks the expansion of multiple malignant B-cell lines and primary mantle-cell lymphoma cells [61]. Our results are consistent with these reports and provide genetic evidence for the importance of targeting both these antioxidant systems for a promising clinical outcome of some B-cell malignancies, where the Trx and the GSH/Grx systems play a pivotal role for cancer sustainment. However, other antioxidant systems, such as xCT and peroxiredoxins, have been also described to be upregulated during lymphocyte differentiation and activation, and to participate in tumor development and propagation [62, 63]. Therefore, efficient interference with the different redox systems for optimal treatment of malignant transformation might depend on the type of lymphoma.

In conclusion, we show that, unlike T cells, B lymphocytes have a surprisingly robust and flexible cellular redox system to sustain thiol-based cellular redox reactions. Deletion of the Trx1 system in B cells leads to a redox rearrangement toward the GSH/Grx1 pathway in order to maintain redox homeostasis and to fuel DNA biosynthesis during B-cell proliferation. These results may impact strategies for therapy of certain B-cell neoplasms.

Materials and methods

Mice

Txnrd1^{fl/fl} mice [15] were provided by M. Conrad (Helmholtz Zentrum, Munich, Germany) and were backcrossed for more than eight generations to C57BL/6. To obtain *Txnrd1^{fl/fl};Cd19-Cre* and *Txnrd1^{fl/fl};Cre-ERT2* mice, *Txnrd1^{fl/fl}* mice were crossed with *Cd19-Cre* [64] and *Cre-ERT2* [65] mice, respectively. B6 *Ptprc^a* (CD45.1) animals were purchased from The Jackson Laboratory (Bar Harbor, Maine, USA). About 6–10 week-old age- and sex-matched mice (either female or male) were used for the experiments. Mice were kept in individually ventilated cages under specific pathogen-free conditions at the ETH Phenomics Center (EPIC; Zurich, Switzerland). All animal experiments were approved by the local animal ethics committee (Kantonales Veterinärdepartement Zürich), licenses ZH054/18 and ZH135/15, and were performed according to local guidelines (TschV, Zurich) and the Swiss animal protection law (TschG). For deletion of the *Txnrd1* gene in *Txnrd1^{fl/fl};Cre-ERT2* mice, animals were intraperitoneally injected with 2 mg TAM (Sigma-Aldrich) on two consecutive days and used for experiments at least 10 days later. For *in vivo* GSH depletion, L-Buthionine-(S,R)-sulfoximine (BSO; Sigma-Aldrich) was supplemented in the drinking water at a concentration of 20 mM for at least 2 weeks as indicated. In addition, animals were intraperitoneally injected with 450 mg/kg of BSO every 2 or 3 days as specified.

Bone marrow chimeras

For bone marrow chimeras, C57BL/6 (CD45.1⁺ CD45.2⁺) recipients were lethally irradiated (9.5 Gy in a RS 2000 [Rad Source Technologies Inc., Alpharetta, USA]) and reconstituted with $1-3 \times 10^6$ bone marrow cells of the donor mice indicated for each experiment. Animals were analyzed 10 weeks after reconstitution.

EdU incorporation

Mice were intraperitoneally injected with 0.5 mg EdU (Life Technologies) and analyzed 12 hours later to compare proliferation of thymocytes with bone marrow cells, or 24 hours later to analyze the homeostatic proliferation of different B-cell populations at steady state. For this purpose, tissues were harvested and treated according to the manufacturer's instructions using the Click-iT Alexa Fluor 488 Imaging Kit (Life Technologies).

Virus infection

Influenza virus strain (A/Puerto Rico/8/34, H1N1) was originally provided by J. Pavlovic, University Zurich. Mice at age of 6–8 weeks were intratracheally infected with either 10 (sublethal

dose) or 500 (lethal dose) plaque-forming units. The body temperature and weight of the mice were monitored daily, and animals were euthanized if they fulfilled severity criteria predefined in the approval of these experiments (ZH135/15) by the local animal ethics committee.

Immunizations

For addressing the response to *Streptococcus pneumoniae*, mice were intravenously injected with 1×10^8 colony-forming units of heat-inactivated pneumococci (strain D36) and were subsequently bled at day 5 to measure IgM antibody responses to phosphorylcholine by ELISA. To analyze GC reactions and antibody production, mice were intraperitoneally injected with 10 μ g of Q β virus-like particles (Q β -VLP) containing *Escherichia coli*-derived RNA. The capsids of the RNA phage Q β were cloned into the pQ β 10 vector and purified as described elsewhere [66, 67].

Cell suspension preparations

Mice were mostly sacrificed by CO₂ asphyxiation. When lungs were harvested for analysis, mice were instead sacrificed by an intraperitoneal overdose of sodium pentobarbital. Organs were removed and processed according to the following procedure. Liver and lungs were minced and then digested for 45 min at 37°C in IMDM medium (Life Technologies) containing 2 mg/mL of type IV collagenase (Worthington) and 0.02 mg/mL DNaseI (Sigma). All other organs were directly disrupted and passed through a 70 μ m cell strainer (Corning). Leukocytes from the liver were isolated by using Percoll gradient centrifugation (GE Healthcare). Bone marrow cells were flushed from femurs and tibia, and then directly passed through the 70 μ m cell strainer. ACK buffer was used for erythrocyte lysis for all organs.

Flow cytometry

For dead cell exclusion, cells were stained with the Zombie Aqua Fixable Viability kit (Biolegend). Prior to surface staining with antibodies, Fc gamma receptors were blocked by incubating cells with anti-CD16/CD32 antibody (2.4G2, homemade). A complete list of all antibodies and staining reagents used in this study can be found in Supporting Information Table 1. Sorting of the different thymocyte populations (ETP, DN1-4, ISP, DP, CD4⁺ SP, and CD8⁺ SP) was performed according to the gating strategy described elsewhere [16]. Cells were acquired on LSRFortessa, or sorted on FACSAria III (BD Bioscience). Data were analyzed in FlowJo software (Tree Star). All the gating strategies used for flow cytometry plots are shown in Supporting Information Figs. 5 and 6. Flow cytometry procedures were in accordance with standard methodological guidelines [68].

Magnetic cell sorting

CD19⁺ B-cell enrichment was achieved by positive selection using a MACS system with microbeads conjugated to monoclonal anti-mouse CD19 (MACS, Miltenyi Biotec) following the manufacturer's instructions.

Glutathione measurement

To measure total GSH levels in cell lysates, the Glutathione Assay Kit (Sigma-Aldrich) was used following the manufacturer's instructions.

Immunohistochemistry staining of cryosections

Freshly isolated spleens were immersed in Tissue-Tek OCT (Sakura) and snap-frozen in liquid nitrogen. Spleen tissue was then cut in 8 μ m sections using a cryostat (Thermo Scientific), and sections were dried overnight. After fixation for 10 min in 100% acetone at 4°C, samples were air-dried and prewet with PBS for 5 min. The sections were blocked using 1% normal mouse serum and 1% BSA for 20 min, and they were then incubated with PNA-biotin (B-1075, Vector Labs) diluted in 1% normal mouse serum and 0.1% BSA for 60 min. Sections were then washed and stained with Q β -VLPs labeled with Alexa Fluor 488 (labeling was performed with the Alexa Fluor 488 labeling kit [A10235, Thermo Fischer Scientific] according to manufacturer's instructions), streptavidin Alexa Fluor 546 (S11225, Thermo Fisher Scientific) and Alexa Fluor 647 rat anti-mouse B220 (557683, BD Pharmingen) for 45 min. Finally, sections were mounted using one drop of Fluoromount G solution (00-4958-02, Thermo Fisher Scientific) and imaged on a Zeiss Axio Imager.A2 microscope using the EC Plan-NEOFLUAR 10x/0.3 objective (ZEISS). Images were acquired using the AxioVision software (ZEISS).

Antibody measurement by ELISA

For measurement of natural antibodies in naïve mice, plates were coated with 1 μ g/mL unlabeled goat anti-mouse IgM, IgG2b, and IgG1 (Southern Biotech). The IgM response to phosphorylcholine was measured by coating plates with 25 μ g/mL of phosphorylcholine conjugated to bovine serum albumin (PC-BSA, Biosearch Technologies). For determination of the antibody response to Q β -VLP, plates were coated with 1 μ g/mL Q β -VLP. For measurement of influenza virus-specific antibodies, plates were coated with UV-inactivated influenza virus (PR8) in PBS. ELISAs were performed according to standard protocols using alkaline phosphatase (AP)-conjugated secondary antibodies: goat anti-mouse IgM, goat anti-mouse IgG1, goat anti-mouse IgG2b (Southern Biotech). The alkaline phosphatase p-nitrophenyl phosphate (pNPP; Sigma-Aldrich) substrate was then added to each well, and the plates were read at 405 nm.

RNA analysis by real-time quantitative PCR

Total RNA was extracted using TRIzol (Life Technologies), followed by reverse transcription using GoScript Reverse Transcriptase (Promega) according to the manufacturer's instructions. Real-time quantitative PCR (RT-PCR) was performed using Brilliant SYBR Green (Stratagene) on an i-Cycler (Bio-Rad Laboratories) according to manufacturer's protocol. Expression was normalized to the housekeeping gene *Tbp* for mRNA expression, or to genomic *Txnrd1* for addressing DNA recombination efficiency in cells lacking the *Txnrd1* gene. The sequences of all used primers are listed in Supporting Information Table 2.

Statistical analysis

Data were analyzed using either a Student's *t* test (two-tailed, unpaired), or one-way ANOVA followed by Tukey's corrections, or two-way ANOVA followed by Bonferroni's corrections. The data are represented as mean + standard deviation or as mean + standard error of mean as indicated in each figure legend. The method of statistical evaluation and the significance levels are also described in each figure legend.

Acknowledgments: We are grateful for research grants from ETH Zurich (ETH-23-16-2) and SNF (310030B-182829). We thank Marcus Conrad for providing *Txnrd1^{fl/fl}* mice. We thank Peter Nielsen, Nike Kräutler, Jan Kisielow, and Luigi Tortola for helpful discussions. We further thank members of the ETH Flow Cytometry Core Facility for cell sorting. We acknowledge the use of the Immgen database as an informative tool for our study.

Author contributions: J.M., H.T., S.H., C.K. performed and analyzed experiments, M.B. and G.B. contributed important reagents and/or technology, J.M. and M.K. designed the study and wrote the manuscript. M.K. obtained funding.

Conflict of interests: The authors declare no commercial or financial conflict of interest.

References

- 1 Stanton, R. C., Glucose-6-phosphate dehydrogenase, NADPH, and cell survival. *IUBMB Life* 2012. **64**: 362–369.
- 2 Arner, E. S. and Holmgren, A., Physiological functions of thioredoxin and thioredoxin reductase. *Eur. J. Biochem.* 2000. **267**: 6102–6109.
- 3 Couto, N., Wood, J. and Barber, J., The role of glutathione reductase and related enzymes on cellular redox homeostasis network. *Free Radic. Biol. Med.* 2016. **95**: 27–42.

- 4 Arner, E. S., Focus on mammalian thioredoxin reductases—important selenoproteins with versatile functions. *Biochim. Biophys. Acta* 2009. **1790**: 495–526.
- 5 Holmgren, A., Thioredoxin. *Annu. Rev. Biochem.* 1985. **54**: 237–271.
- 6 Holmgren, A., Antioxidant function of thioredoxin and glutaredoxin systems. *Antioxid. Redox Signal.* 2000. **2**: 811–820.
- 7 Prinz, W. A., Aslund, F., Holmgren, A. and Beckwith, J., The role of the thioredoxin and glutaredoxin pathways in reducing protein disulfide bonds in the *Escherichia coli* cytoplasm. *J. Biol. Chem.* 1997. **272**: 15661–15667.
- 8 Mustacich, D. and Powis, G., Thioredoxin reductase. *Biochem. J.* 2000. **346**(Pt 1): 1–8.
- 9 Lu, S. C., Glutathione synthesis. *Biochim. Biophys. Acta* 2013. **1830**: 3143–3153.
- 10 Lillig, C. H. and Holmgren, A., Thioredoxin and related molecules—from biology to health and disease. *Antioxid. Redox Signal.* 2007. **9**: 25–47.
- 11 Holmgren, A. and Sengupta, R., The use of thiols by ribonucleotide reductase. *Free Radic. Biol. Med.* 2010. **49**: 1617–1628.
- 12 Potamitou, A., Holmgren, A. and Vlamis-Gardikas, A., Protein levels of *Escherichia coli* thioredoxins and glutaredoxins and their relation to null mutants, growth phase, and function. *J. Biol. Chem.* 2002. **277**: 18561–18567.
- 13 Camier, S., Ma, E., Leroy, C., Pruvost, A., Toledano, M. and Marsolier-Kergoat, M. C., Visualization of ribonucleotide reductase catalytic oxidation establishes thioredoxins as its major reductants in yeast. *Free Radic. Biol. Med.* 2007. **42**: 1008–1016.
- 14 Bondareva, A. A., Capecchi, M. R., Iverson, S. V., Li, Y., Lopez, N. I., Lucas, O., Merrill, G. F. et al., Effects of thioredoxin reductase-1 deletion on embryogenesis and transcriptome. *Free Radic. Biol. Med.* 2007. **43**: 911–923.
- 15 Jakupoglu, C., Przemeck, G. K., Schneider, M., Moreno, S. G., Mayr, N., Hatzopoulos, A. K., de Angelis, M. H. et al., Cytoplasmic thioredoxin reductase is essential for embryogenesis but dispensable for cardiac development. *Mol. Cell. Biol.* 2005. **25**: 1980–1988.
- 16 Muri, J., Heer, S., Matsushita, M., Pohlmeier, L., Tortola, L., Fuhrer, T., Conrad, M. et al., The thioredoxin-1 system is essential for fueling DNA synthesis during T-cell metabolic reprogramming and proliferation. *Nat. Commun.* 2018. **9**: 1851.
- 17 Prigge, J. R., Eriksson, S., Iverson, S. V., Meade, T. A., Capecchi, M. R., Arner, E. S. and Schmidt, E. E., Hepatocyte DNA replication in growing liver requires either glutathione or a single allele of *txnrd1*. *Free Radic. Biol. Med.* 2012. **52**: 803–810.
- 18 Eriksson, S., Prigge, J. R., Talago, E. A., Arner, E. S. and Schmidt, E. E., Dietary methionine can sustain cytosolic redox homeostasis in the mouse liver. *Nat. Commun.* 2015. **6**: 6479.
- 19 Prigge, J. R., Coppo, L., Martin, S. S., Ogata, F., Miller, C. G., Bruschwein, M. D., Orlicky, D. J. et al., Hepatocyte hyperproliferation upon liver-specific co-disruption of thioredoxin-1, thioredoxin reductase-1, and glutathione reductase. *Cell Rep.* 2017. **19**: 2771–2781.
- 20 Buck, M. D., Sowell, R. T., Kaech, S. M. and Pearce, E. L., Metabolic instruction of immunity. *Cell* 2017. **169**: 570–586.
- 21 Buck, M. D., O'Sullivan, D. and Pearce, E. L., T cell metabolism drives immunity. *J. Exp. Med.* 2015. **212**: 1345–1360.
- 22 Wang, R., Dillon, C. P., Shi, L. Z., Milasta, S., Carter, R., Finkelstein, D., McCormick, L. L. et al., The transcription factor Myc controls metabolic reprogramming upon T lymphocyte activation. *Immunity* 2011. **35**: 871–882.

- 23 Blair, D., Dufort, F. J. and Chiles, T. C., Protein kinase C β is critical for the metabolic switch to glycolysis following B-cell antigen receptor engagement. *Biochem. J.* 2012. **448**: 165–169.
- 24 Doughty, C. A., Bleiman, B. F., Wagner, D. J., Dufort, F. J., Mataraza, J. M., Roberts, M. F. and Chiles, T. C., Antigen receptor-mediated changes in glucose metabolism in B lymphocytes: role of phosphatidylinositol 3-kinase signaling in the glycolytic control of growth. *Blood* 2006. **107**: 4458–4465.
- 25 Ganeshan, K. and Chawla, A., Metabolic regulation of immune responses. *Annu. Rev. Immunol.* 2014. **32**: 609–634.
- 26 Hardy, R. R., Carmack, C. E., Shinton, S. A., Kemp, J. D. and Hayakawa, K., Resolution and characterization of pro-B and pre-pro-B cell stages in normal mouse bone marrow. *J. Exp. Med.* 1991. **173**: 1213–1225.
- 27 Pillai, S. and Cariappa, A., The follicular versus marginal zone B lymphocyte cell fate decision. *Nat. Rev. Immunol.* 2009. **9**: 767–777.
- 28 Baumgarth, N., The double life of a B-1 cell: self-reactivity selects for protective effector functions. *Nat. Rev. Immunol.* 2011. **11**: 34–46.
- 29 Holodick, N. E., Rodriguez-Zhurbenko, N. and Hernandez, A. M., Defining natural antibodies. *Front Immunol.* 2017. **8**: 872.
- 30 Martin, F., Oliver, A. M. and Kearney, J. F., Marginal zone and B1 B cells unite in the early response against T-independent blood-borne particulate antigens. *Immunity* 2001. **14**: 617–629.
- 31 Tanigaki, K., Han, H., Yamamoto, N., Tashiro, K., Ikegawa, M., Kuroda, K., Suzuki, A. et al., Notch-RBP-J signaling is involved in cell fate determination of marginal zone B cells. *Nat. Immunol.* 2002. **3**: 443–450.
- 32 Baumgarth, N., B-1 cell heterogeneity and the regulation of natural and antigen-induced IgM production. *Front Immunol.* 2016. **7**: 324.
- 33 Griffith, O. W. and Meister, A., Potent and specific inhibition of glutathione synthesis by buthionine sulfoximine (S-n-butyl homocysteine sulfoximine). *J. Biol. Chem.* 1979. **254**: 7558–7560.
- 34 Watanabe, T., Sagisaka, H., Arakawa, S., Shibaya, Y., Watanabe, M., Igarashi, I., Tanaka, K. et al., A novel model of continuous depletion of glutathione in mice treated with L-buthionine (S,R)-sulfoximine. *J. Toxicol. Sci.* 2003. **28**: 455–469.
- 35 Bachmann, M. F., Hengartner, H. and Zinkernagel, R. M., T helper cell-independent neutralizing B cell response against vesicular stomatitis virus: role of antigen patterns in B cell induction? *Eur. J. Immunol.* 1995. **25**: 3445–3451.
- 36 Bachmann, M. F. and Zinkernagel, R. M., Neutralizing antiviral B cell responses. *Annu. Rev. Immunol.* 1997. **15**: 235–270.
- 37 Jegerlehner, A., Maurer, P., Bessa, J., Hinton, H. J., Kopf, M. and Bachmann, M. F., TLR9 signaling in B cells determines class switch recombination to IgG2a. *J. Immunol.* 2007. **178**: 2415–2420.
- 38 Jennings, G. T. and Bachmann, M. F., The coming of age of virus-like particle vaccines. *Biol. Chem.* 2008. **389**: 521–536.
- 39 Victora, G. D., Schwickert, T. A., Fooksman, D. R., Kamphorst, A. O., Meyer-Hermann, M., Dustin, M. L. and Nussenzweig, M. C., Germinal center dynamics revealed by multiphoton microscopy with a photoactivatable fluorescent reporter. *Cell* 2010. **143**: 592–605.
- 40 Fox, C. J., Hammerman, P. S. and Thompson, C. B., Fuel feeds function: energy metabolism and the T-cell response. *Nat. Rev. Immunol.* 2005. **5**: 844–852.
- 41 Pearce, E. L. and Pearce, E. J., Metabolic pathways in immune cell activation and quiescence. *Immunity* 2013. **38**: 633–643.
- 42 van der Windt, G. J. and Pearce, E. L., Metabolic switching and fuel choice during T-cell differentiation and memory development. *Immunol. Rev.* 2012. **249**: 27–42.
- 43 Wang, R. and Green, D. R., Metabolic checkpoints in activated T cells. *Nat. Immunol.* 2012. **13**: 907–915.
- 44 Dufort, F. J., Bleiman, B. F., Gumina, M. R., Blair, D., Wagner, D. J., Roberts, M. F., Abu-Amer, Y. et al., Cutting edge: IL-4-mediated protection of primary B lymphocytes from apoptosis via Stat6-dependent regulation of glycolytic metabolism. *J. Immunol.* 2007. **179**: 4953–4957.
- 45 Mak, T. W., Grusdat, M., Duncan, G. S., Dostert, C., Nonnenmacher, Y., Cox, M., Binsfeld, C. et al., Glutathione primes T cell metabolism for inflammation. *Immunity* 2017. **46**: 675–689.
- 46 Gatto, D., Bauer, M., Martin, S. W. and Bachmann, M. F., Heterogeneous antibody repertoire of marginal zone B cells specific for virus-like particles. *Microbes Infect.* 2007. **9**: 391–399.
- 47 Bertolotti, M., Sitia, R. and Rubartelli, A., On the redox control of B lymphocyte differentiation and function. *Antioxid. Redox Signal.* 2012. **16**: 1139–1149.
- 48 Aronov, M. and Tirosh, B., Metabolic control of plasma cell differentiation—what we know and what we don't know. *J. Clin. Immunol.* 2016. **36**(Suppl 1): 12–17.
- 49 Bertolotti, M., Yim, S. H., Garcia-Manteiga, J. M., Masciarelli, S., Kim, Y. J., Kang, M. H., Iuchi, Y. et al., B- to plasma-cell terminal differentiation entails oxidative stress and profound reshaping of the antioxidant responses. *Antioxid. Redox Signal.* 2010. **13**: 1133–1144.
- 50 Arner, E. S. and Holmgren, A., The thioredoxin system in cancer. *Semin. Cancer Biol.* 2006. **16**: 420–426.
- 51 Karlenius, T. C. and Tonissen, K. F., Thioredoxin and cancer: a role for thioredoxin in all states of tumor oxygenation. *Cancers* 2010. **2**: 209–232.
- 52 Powis, G. and Kirkpatrick, D. L., Thioredoxin signaling as a target for cancer therapy. *Curr. Opin. Pharmacol.* 2007. **7**: 392–397.
- 53 Hanahan, D. and Weinberg, R. A., The hallmarks of cancer. *Cell* 2000. **100**: 57–70.
- 54 Tonissen, K. F. and Di Trapani, G., Thioredoxin system inhibitors as mediators of apoptosis for cancer therapy. *Mol. Nutr. Food Res.* 2009. **53**: 87–103.
- 55 Urig, S. and Becker, K., On the potential of thioredoxin reductase inhibitors for cancer therapy. *Semin. Cancer Biol.* 2006. **16**: 452–465.
- 56 Marzano, C., Gandin, V., Folda, A., Scutari, G., Bindoli, A. and Rigobello, M. P., Inhibition of thioredoxin reductase by auranofin induces apoptosis in cisplatin-resistant human ovarian cancer cells. *Free Radic. Biol. Med.* 2007. **42**: 872–881.
- 57 Kim, N. H., Park, H. J., Oh, M. K. and Kim, I. S., Antiproliferative effect of gold(I) compound auranofin through inhibition of STAT3 and telomerase activity in MDA-MB 231 human breast cancer cells. *BMB Rep.* 2013. **46**: 59–64.
- 58 Nakaya, A., Sagawa, M., Muto, A., Uchida, H., Ikeda, Y. and Kizaki, M., The gold compound auranofin induces apoptosis of human multiple myeloma cells through both down-regulation of STAT3 and inhibition of NF- κ B activity. *Leuk. Res.* 2011. **35**: 243–249.
- 59 Harris, I. S., Treloar, A. E., Inoue, S., Sasaki, M., Gorrini, C., Lee, K. C., Yung, K. Y. et al., Glutathione and thioredoxin antioxidant pathways synergize to drive cancer initiation and progression. *Cancer Cell* 2015. **27**: 211–222.
- 60 Mandal, P. K., Schneider, M., Kolle, P., Kuhlencordt, P., Forster, H., Beck, H., Bornkamm, G. W. and Conrad, M., Loss of thioredoxin reductase 1 renders tumors highly susceptible to pharmacologic glutathione deprivation. *Cancer Res.* 2010. **70**: 9505–9514.
- 61 Kiebal, M., Skalska, J., Casulo, C., Brookes, P. S., Peterson, D. R., Hilchey, S. P., Dai, Y. et al., Dual targeting of the thioredoxin and glutathione

- antioxidant systems in malignant B cells: a novel synergistic therapeutic approach. *Exp. Hematol.* 2015. **43**: 89–99.
- 62 Dai, L., Cao, Y., Chen, Y., Kaleeba, J. A., Zabaleta, J. and Qin, Z., Genomic analysis of xCT-mediated regulatory network: identification of novel targets against AIDS-associated lymphoma. *Oncotarget* 2015. **6**: 12710–12722.
- 63 Trzeciacka, A., Klossowski, S., Bajor, M., Zagodzón, R., Gaj, P., Muchowicz, A., Malinowska, A. et al., Dimeric peroxiredoxins are druggable targets in human Burkitt lymphoma. *Oncotarget* 2016. **7**: 1717–1731.
- 64 Rickert, R. C., Roes, J. and Rajewsky, K., B lymphocyte-specific, Cre-mediated mutagenesis in mice. *Nucleic. Acids. Res.* 1997. **25**: 1317–1318.
- 65 Hameyer, D., Loonstra, A., Eshkind, L., Schmitt, S., Antunes, C., Groen, A., Bindels, E. et al., Toxicity of ligand-dependent Cre recombinases and generation of a conditional Cre deleter mouse allowing mosaic recombination in peripheral tissues. *Physiol. Genomics* 2007. **31**: 32–41.
- 66 Cielens, I., Ose, V., Petrovskis, I., Strelnikova, A., Renhofa, R., Kozlovskaya, T. and Pumpens, P., Mutilation of RNA phage Qbeta virus-like particles: from icosahedrons to rods. *FEBS Lett.* 2000. **482**: 261–264.
- 67 Storni, T., Lechner, F., Erdmann, I., Bachi, T., Jegerlehner, A., Dumrese, T., Kundig, T. M. et al., Critical role for activation of antigen-presenting cells in priming of cytotoxic T cell responses after vaccination with virus-like particles. *J. Immunol.* 2002. **168**: 2880–2886.
- 68 Cossarizza, A., Chang, H. D., Radbruch, A., Akdis, M., Andra, I., Annunziato, F., Bacher, P. et al., Guidelines for the use of flow cytometry and cell sorting in immunological studies. *Eur. J. Immunol.* 2017. **47**: 1584–1797.

Abbreviations: BSO: buthionine-sulfoximine · GC: germinal center · GSH: glutathione · MZ: marginal zone · NOX: NADPH oxidases · OXPHOS: oxidative phosphorylation · PPP: pentose phosphate pathway · TAM: tamoxifen · VLP: virus-like particle

Full correspondence: Prof. Manfred Kopf, Institute of Molecular Health Sciences, ETH Zürich, Otto-Stern-Weg 7, 8093 Zürich, Switzerland
e-mail: Manfred.Kopf@ethz.ch

The peer review history for this article is available at
<https://publons.com/publon/10.1002/eji.201848044>

Received: 3/12/2018

Revised: 22/1/2019

Accepted: 22/2/2019

Accepted article online: 25/2/2019